

Spectral Distribution Dynamics across Different Attentional Priority States

Mattia Pietrelli,¹ Jason Samaha,² and Bradley R. Postle^{1,3}

¹Department of Psychiatry, University of Wisconsin–Madison, Madison, Wisconsin 53719, ²Department of Psychology, University of California, Santa Cruz, California 95064, and ³Department of Psychology, University of Wisconsin–Madison, Madison, Wisconsin 53706

Anticipatory covert spatial attention improves performance on tests of visual detection and discrimination, and shifts are accompanied by decreases and increases of α band power at electroencephalography (EEG) electrodes corresponding to the attended and unattended location, respectively. Although the increase at the unattended location is often interpreted as an active mechanism (e.g., inhibiting processing at the unattended location), most experiments cannot rule out the alternative possibility that it is a secondary consequence of selection elsewhere. To adjudicate between these accounts, we designed a Posner-style visual cueing task in which male and female human participants made orientation judgments of targets appearing at one of four locations: up, down, right, or left. Critically, trials were blocked such that within a block the locations along one meridian alternated in status between attended and unattended, and targets never appeared at the other two, making them irrelevant. Analyses of the concurrently measured EEG signal were conducted on “traditional” narrowband α (8–14 Hz), as well as on two components resulting from the decomposition of this signal: “periodic” α ; and the slope of the aperiodic 1/f-like component. Although data from right-left blocks replicated the familiar pattern of lateralized asymmetry in narrowband α power, with neither α signal could we find evidence for any difference in the time course at unattended versus irrelevant locations, an outcome consistent with the secondary-consequence interpretation of attention-related dynamics in the α band. Additionally, 1/f slope was shallower at attended and unattended locations, relative to irrelevant, suggesting a tonic adjustment of physiological state.

Key words: α oscillation; aperiodic component; irrelevant location; LASSO; multivariate analysis; spatial attention

Significance Statement

Visual spatial attention, the prioritization of one location in the visual field, is critical for guiding behavior in cluttered environments. Although influential theories posit an important role for α band oscillations in the inhibition of processing at unattended locations, we used a novel procedure to find evidence for an alternative interpretation: selection of one location may simply result in a return to physiological baseline at all others. In addition to determining one way that attention does not work (important for future progress in this field), we also discovered novel evidence for one way that it does work: by modifying the tonic physiological state (indexed by an aperiodic component of the electroencephalography (EEG)) at locations where spatial selection is likely to occur.

Received Nov. 22, 2021; revised Mar. 31, 2022; accepted Apr. 2, 2022.

Author contributions: M.P., J.S., and B.R.P. designed research; M.P. performed research; M.P. analyzed data; M.P. wrote the first draft of the paper; M.P., J.S., and B.R.P. edited the paper; M.P. and B.R.P. wrote the paper.

Citation Gender Diversity Statement: A retrospective analysis of citation patterns in five broad scope neuroscience journals over the past 25 years has revealed a persistent pattern of gender imbalance: although the proportions of authorship teams (categorized by estimated gender identification of first author/last author) publishing in these journals in 2018 were M(an)/M = 0.50, W(oman)/M = 0.27, M/W = 0.13, and W/W = 0.10, the comparable proportions for the articles that these authorship teams cited were M/M = 0.617, W/M = 0.236, M/W = 0.09, and W/W = 0.058 (Dworkin et al., 2020). Using a similar method, we estimate the citations by gender category of this paper to be: M/M = 0.81, W/M = 0.071, M/W = 0.095, and W/W = 0.024.

This work was supported by the National Institutes of Health Grant MH095084 (to B.R.P.).

The authors declare no competing financial interests.

Correspondence should be addressed to Bradley R. Postle at postle@wisc.edu.

<https://doi.org/10.1523/JNEUROSCI.2318-21.2022>

Copyright © 2022 the authors

Introduction

Valid expectations about where a visual stimulus will appear improve performance on tests of visual detection and discrimination (Posner, 1980). With electroencephalography (EEG) the onset of a spatial cue triggers a decrease in the power of oscillations in the α band (\sim 8–14 Hz; henceforth “ α ”) at posterior electrodes contralateral to the cued location, and a commensurate increase in α power at electrodes ipsilateral to the cued location (Thut et al., 2006; Rihs et al., 2009; Capilla et al., 2014). However, consensus is lacking about the functional interpretation of this familiar pattern: are these attention-related changes in α dynamics reflective of active mechanisms that implement attentional control (Sadaghiani and Kleinschmidt, 2016), or are they byproducts of attention-related state changes that were caused by

other mechanisms (i.e., a “secondary consequence”; Antonov et al., 2020)? As an example of an active mechanism, one influential account holds that the increase in power at “unattended electrodes” reflects the active inhibition of processing at that location, presumably to suppress the processing of distracting information (Kelly et al., 2006; Jensen and Mazaheri, 2010). Alternatively, a “secondary-consequence” account interprets this same effect as a consequence of the withdrawal of attention (Foster and Awh, 2019; Antonov et al., 2020). An analogy for the secondary-consequence account is eye closing, for which the increase in power of posterior α is a consequence of the loss of visual input, not the operation of a mechanism that caused eyelid closure.

To adjudicate between these accounts, we modified the standard spatial-cueing procedure, which compares attended versus unattended locations, to create a third class of locations: locations that would never be cued during a block of trials, i.e., irrelevant locations. On any block of trials, targets would only appear along one axis (e.g., to the left or right of fixation), but never along the other axis (in this example, above or below fixation), thereby making above and below irrelevant during this block of trials. If the increase in α power at the unattended location reflects an active mechanism, it should not be observed at the irrelevant locations, e.g., in the motor control, memory, and working memory literature, focal increases in α power are found when top-down inhibitory control is needed to withhold or otherwise control the execution of a response to an otherwise prepotent location (Klimesch et al., 2007; Jensen and Mazaheri, 2010; irrelevant areas should not have such prepotency). If, alternatively, the increase in α power at the unattended location is a secondary consequence of the selection of a different location, irrelevant locations might also experience a return to a baseline state.

One potential concern about our design is that one of the two accounts, secondary consequence, predicts the absence of evidence for a statistical difference between unattended and irrelevant α power. Therefore, were this to be the outcome, we planned to assess whether some other component in the same data does discriminate unattended from irrelevant. More specifically, we planned to decompose the EEG data into periodic and aperiodic components. Although task-related modulation in a predefined frequency band (e.g., α) is most often interpreted as a change in the power of an oscillator, at least some of that change might be the result any of several other factors, including a change of the center of frequency of an oscillator (Haegens et al., 2014; Mierau et al., 2017), a change of the bandwidth of an oscillator, or a change in the $1/f$ -like aperiodic component on which the power from the true oscillator sits (Voytek et al., 2015; Donoghue et al., 2020a). Because these factors are mathematically independent, it is possible that the neural generators underlying them may also vary independently. Consequently, if “traditional α ,” generated with bandpass-filtering, failed to discriminate unattended locations from irrelevant ones, we reasoned that perhaps one of these decomposed components of the EEG signal would be successful.

Materials and Methods

Subjects

Nineteen healthy subjects (8 males and 11 females; age $M = 22.6$, $S = 4.7$) were recruited from the University of Wisconsin–Madison community and were compensated monetarily. This study sample size was based on previous studies that have influenced our thinking about attention-related α dynamics (Thut et al., 2006; Rihs et al., 2009), to facilitate contextualization of our findings with them. All subjects reported

right-handedness and normal or corrected-to-normal visual acuity and color vision. None reported any medical, neurologic, or psychiatric disorder. The University of Wisconsin–Madison Health Sciences Institutional Review Board approved the study.

Experimental design

The task was a two-alternative forced-choice discrimination of orientation, between Gabor patches oriented 45° clockwise or counterclockwise, with a symbolic cue preceding the target and carrying information about where and when the target would appear. Trials were administered in alternating 70-trial blocks in which target stimuli appeared exclusively at a location 7.5 degrees of visual angle (DVA) to the left or to the right of central fixation (2°), or exclusively 7.5 DVA above or below fixation. Overall, subjects completed five horizontal and five vertical blocks (Fig. 1), for a total of 700 trials per subject.

Experimental procedure

Subjects completed the experiment in one session, while seated in an acoustically shielded and dimly lit room. Stimulus presentation was controlled with MATLAB (2020b, The MathWorks) and presented on a 53×30 cm screen (refresh rate, 60 Hz) at a viewing distance of ~ 57 cm. Throughout the experiment, the background screen was gray. Before the 10 experimental blocks, each subject first completed a titration procedure to determine presentation parameters that produced discrimination performance near 75% accuracy, then a training block using those parameters. For clarity, the titration procedure and training block will be described after the description of the main experiment.

In the main experiment (Fig. 1), each trial started with the presentation of a fixation cross for 1000–1500 ms (randomly picked with 100-ms steps), replaced by the 200-ms presentation of a symbolic cue (an arrowhead) in the center of the screen. The direction of the arrow indicated the location of the forthcoming target with 75% validity; on the remaining 25% of trials the target appeared in the opposite location on the same meridian. The color of the arrow contained information about the cue-to-target interval (CTI): a magenta arrow indicated, with 100% validity, a CTI of 650 ms, whereas a green arrow indicated that the CTI could come from one of four durations (650, 900, 1150, 1400 ms) drawn randomly from an exponential distribution. From the full set of 700 trials, only the 400 trials with a CTI of 650 ms were used for the analyses reported here. The reason for including trials with CTI durations longer than 650 ms was to make it difficult for participants to estimate the hazard function of target onset time. Data from CTIs longer than 650 ms would have progressively worse SNR (because of fewer observations), and analyses including longer trials would be complicated by the discontinuity of timepoints between trials.

The cue was replaced by a white fixation cross, then the target (50 ms), then a backward mask (50 ms). The target was a Gabor patch, 80×80 pixels ($\sim 2^\circ$) in size, with spatial frequency of one cycle every 10 pixels, oriented either 45° clockwise or counterclockwise of vertical. Novel masks were generated for each trial by filling in a circular aperture the size of the Gabor with randomly arranged black and white pixels. Subjects were instructed to make a clockwise/counterclockwise orientation discrimination of each target, and to register their decision as quickly and accurately as possible by pressing the left arrow key on a keyboard for a counterclockwise orientation (index finger of right hand) and the right arrow key for a clockwise orientation (middle finger of right hand). After each orientation response, subjects then rated the subjective visibility of the target, using the perceptual awareness scale (PAS) rating (Ramsoy and Overgaard, 2004): the sentence “Perceptual awareness rating?” was presented, along with the digits “1,” “2,” “3,” and “4,” and subjects indicated their rating by selecting the corresponding key on the keyboard with their left hand. Subjects were instructed to press “1” when they had no subjective experience of seeing the target; to press “2” when they perceived a distinction between target and mask, but did not perceive the target’s orientation; to press “3” when they had an impression that they had perceived the target, but that it was not clearly visible; and to press four when they were confident that they had seen the target clearly. For this, subjects were asked to “think carefully” about their visibility rating, and to take as much time as they needed before responding.

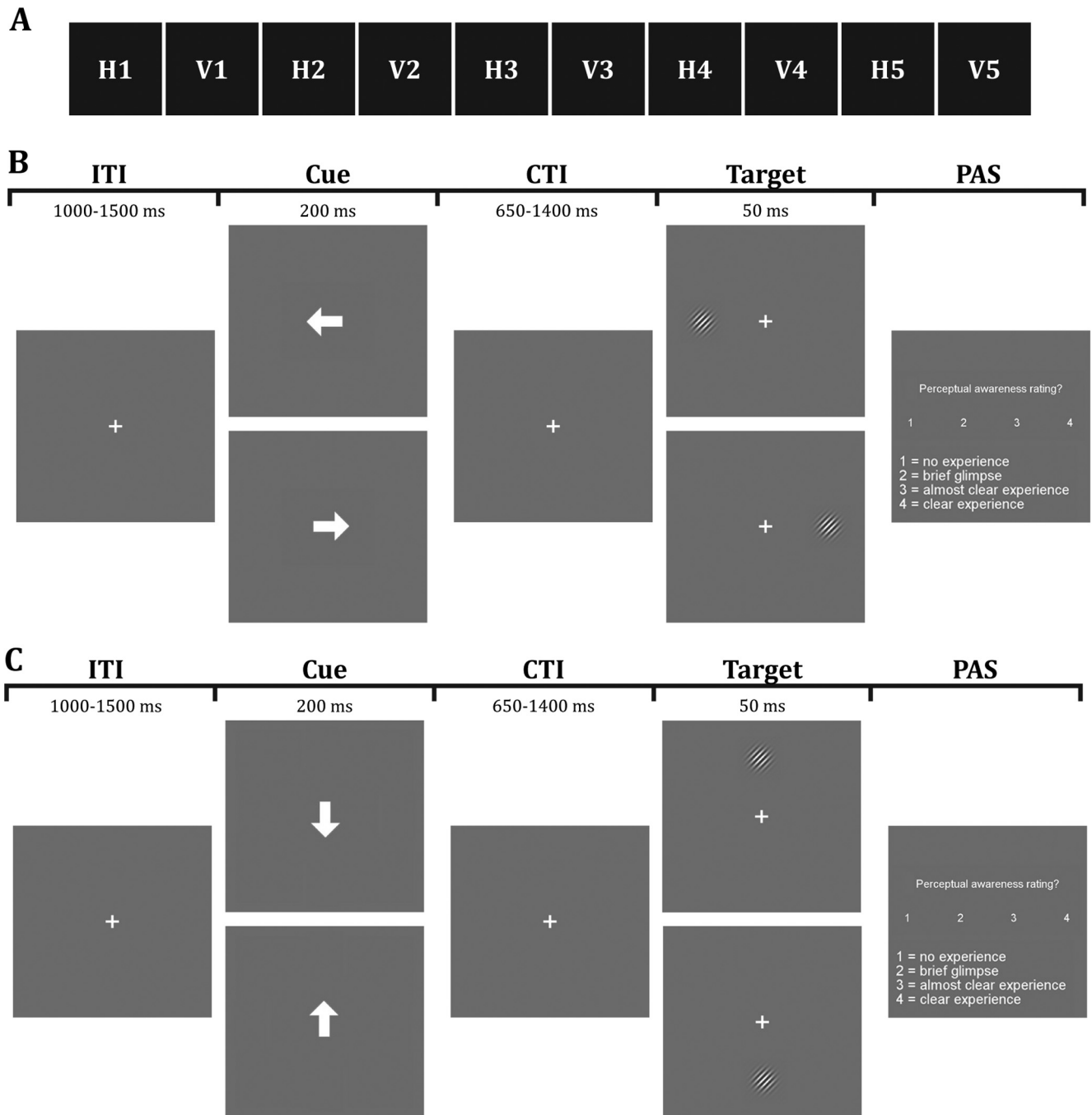


Figure 1. Visual representation of the experimental design. **A**, Progression of block types through the experimental procedure, alternating horizontal and vertical blocks (H = horizontal block, V = vertical block). **B**, Time course of horizontal trials, where the cue can only point to the right or left, and the target can be presented just to right or left to the fixation cross. **C**, Trial course of vertical trials, where the cue can only point down or up, and the target can be presented just below or above the fixation cross (ITI = intertrial interval, CTI = cue-to-target interval, PAS = perceptual awareness rating).

In order to validate this aspect of the procedure, no target was present on 20% of trials (just a black 80×80 patch without any stripe for 50 ms, followed by the 50-ms backward mask).

Inferential statistical analyses of the behavioral data were performed using STATISTICA (version 12.0; StatSoft), and *post hoc* comparisons were conducted using Newman–Keuls tests.

Titration procedure

Before the main experiment, each subject completed two runs through a titration procedure, one for vertical and one for horizontal locations, during which the contrast level of the target was gradually varied to obtain a discrimination accuracy of 75%, using the QUEST adaptive

staircase procedure (Watson and Pelli, 1983; King-Smith et al., 1994). Specifically, each run began with a contrast level of 75% (highly visible) and the contrast on each subsequent trial was adjusted up or down, in steps of 2%, depending on the accuracy of the previous trial. QUEST uses Bayes' theorem to estimate the response of the actual trial based on the history of past trials, to calculate the psychometric function for contrast detection. Each run contained 80 trials, 40 for each target position tested, consequently, a perceptual threshold of 75% orientation discrimination accuracy was estimated independently for each of the four locations (Contrast values: up 48.0%, right 39.0%, down 43.0%, left 45.9%). Each trial of the titration runs was identical to the experimental blocks, except no symbolic cue was presented, no visibility report was requested, and feedback was provided after each response.

Training procedure

After titration, subjects received instruction via progressive introduction (from the trial structure of the titration procedure) to elements from the experimental task, using the contrast level previously found during the titration procedure. First, they were instructed about the meaning of the direction of the cue and performed 20 trials with a white cue. Next, they were instructed about the meaning of the color of the cue and performed 20 additional trials with the cue containing both the location and timing information. Finally, they were instructed on how to respond on the PAS, and during 40 remaining trials the visibility rating screen was presented after each orientation response.

EEG recording and preprocessing

EEG signal was recorded from 60 Ag/AgCl electrodes with positions conforming to the extended 10–20 international system. Recordings were made using a forehead reference electrode and amplified with an Eximia 60-channel amplifier (Nextim) with a sampling rate of 1450 Hz. Preprocessing and analysis were conducted with MATLAB (2020b, The MathWorks) using custom routines and EEGLAB (v. 2019/1) toolbox (Delorme and Makeig, 2004). Data were down-sampled offline to 1000 Hz and were divided into epochs ranging between -1000 to $+1400$ ms around cue onset. Epochs with muscle artifacts were identified by a trained operator and discarded ($M = 2.3\%$, $STD = 4.0\%$). After reducing data dimensionality to 32 components based on principal component analysis, horizontal and vertical eye-movement artifacts were visually identified and removed by means of independent component analysis (ICA) by a trained operator ($M = 1.0\%$, $STD = 0.7\%$).

Time-frequency and periodic/aperiodic decomposition

From the cleaned data, a complex Morlet wavelet decomposition (Cohen, 2019) was applied to each single epoch (1–50 Hz, 0.35 Hz frequencies bins, 3–10 cycles) with a custom routine in the Fieldtrip toolbox environment (Oostenveld et al., 2011; version 2021/03/11). The resultant time-frequency series were down-sampled from 1800 (1000 Hz) to 200 (111 Hz) timepoints, to reduce processing time for subsequent analyses. In order to track α power activity across the different attentional priority conditions, power values were averaged across the α band interval 8–14 Hz (Thut et al., 2006; Rihs et al., 2009) and baseline corrected (by subtraction) to the average across all trials of the precue period between -500 and 0 ms. It is on these data, from here forward “narrowband α power,” that we conducted the analyses intended to adjudicate between inhibition versus idling accounts of α dynamics during spatial cueing (i.e., the time window for the signal of interest was the entire trial, from -500 to 1300 ms relative to cue onset).

After analyzing the narrowband α power data, we decomposed the EEG data into putatively oscillatory and aperiodic components by carrying out a parametrization of the spectral distribution with the fitting-oscillations-and-one-over-f (FOOOF) toolbox (Donoghue et al., 2020b). For each subject, a FOOOF routine was run on the time-frequency series, estimating the aperiodic-adjusted power at the peak of α and the slope of the $1/f$ aperiodic component of the spectral distribution, separately for each electrode, each trial, and each time point. This procedure was run across the frequency range 3.33–50 Hz with three frequency values per Hertz, and the following parameters: peak width limits: 1–8; max number of peaks: 6; minimum peak height: 0.05; peak threshold: 1.5; and aperiodic mode: “fixed.” Finally, the estimated aperiodic-adjusted power at the peak of α and the slope of the $1/f$ aperiodic component values were baseline corrected (by subtraction) to the across-trial average of the precue period between -500 and 0 ms, to produce what we will refer to as “decomposed α power” and “ $1/f$ slope.” For clarity, note that greater $1/f$ slope values indicate a steeper aperiodic component, while lower $1/f$ slope values indicate a shallower aperiodic component.

Electrode selection

The main challenge of our procedure was the need to isolate signals selective for each of the four target locations. In particular, for the selection of electrodes corresponding to “up” and “down” locations on the vertical meridian there is not a procedure analogous to selecting a

stereotypical set of contralateral electrodes, as is typically done for tasks using only left and right locations. Our solution to this challenge was use a data-driven, multivariate procedure to identify electrodes that preferentially represent just one location. One method, multivariate inverted encoding modeling (mIEM), can be used to reconstruct (effectively, “decode”) attended locations at any polar angle relative to fixation from a 64D EEG dataset (Samaha et al., 2016). However, this method does not offer a principled way to cut off the number of electrodes considered to be selective for each location. For this reason, our first choice method was to use classification via L1-regularized logistic regression (from now, LASSO; Tibshirani, 1996), because the loss function of its regularization procedure maximizes the contribution of location-informative features (here, channels) while pushing to zero the contribution of nonrelevant and redundant features (Tibshirani, 1996). That is, LASSO offers an objective method for electrode selection. One complication that can arise, however, is that for some datasets LASSO’s solution can be to reduce the number of selected features to 0. In these instances (i.e., when LASSO failed to identify a set of electrodes selective for a location), we would use mIEM and select, for each location, the number of electrodes from the β coefficient matrix corresponding to the average size of regions of interest (ROIs) identified with LASSO.

It is important to note that, by adopting this approach, we forwent the ability to draw any inferences about what might be the cortical sources of the signals we would be analyzing. This is because neither LASSO nor mIEM are constrained by an electrode’s location on the scalp, and so the ROIs constructed with the results of their analyses (see below, A priori ROIs) would be likely, for example, to include nonadjacent electrodes.

A priori ROIs

Before hypothesis testing, to determine whether our data replicated established findings, we constructed a priori ROIs to isolate signal corresponding to left (P8, P10, and O2) and right (P7, P9, and O1) target locations (Thut et al., 2006; Rihs et al., 2009). Figure 2 illustrates that, with these a priori ROIs, data from horizontal blocks showed only a numerical trend toward the expected pattern of greater narrowband α power at electrodes corresponding to unattended than attended locations during the CTI, and that this effect became significant only a few hundred milliseconds after Target onset. On its face, this may seem to not replicate earlier reports of attention-related lateralization of α power during the CTI (Thut et al., 2006; Rihs et al., 2009). However, it is important to note that the CTIs in those studies were markedly longer (2.6 s in Thut et al., 2006; and 1900 ms in Rihs et al., 2009), and in both of these studies the evidence for lateralized differences was markedly stronger during the second half of these long CTIs. (Inspection of Rihs et al., 2009, their Fig. 3, for example, reveals marked reductions in α power bilaterally in the 500- to 700-ms window, on both Cue R and Cue L trials, and only in the 700- to 900-ms window is the lateralized attention effect clearly visible.) Visual inspection of the data from Figure 2 was used to select the time interval of 1000–1200 ms with which to train classifiers to identify the electrodes for construction of up, right, down, and left ROIs.

L1-regularized logistic regression classifier

In order to identify which (and how many) electrodes preferentially represented each of the four target locations (up, right, down, and left) we classified the data at each electrode during the target window (1000–1200 ms) with LASSO. (The same procedure was followed to create ROIs defined with data corresponding to narrowband α power, decomposed α power, and $1/f$ slope.) For each of the four target locations, the contribution of each electrode was logistically regressed to classify the tested location against the nontested locations, using the least squares algorithm to select location-selective electrodes by shrinking the contribution of noninformative or redundant channels to 0 (Tibshirani, 1996).

For each participant, each location (the target on ~ 100 trials) was classified against nontarget locations (~ 100 trials \times three locations) with a nested cross-validation procedure. The outer loop was used for estimating the quality of the models trained in the inner loop, with a leave-one-trial-out cross-validation procedure. The inner loop was used

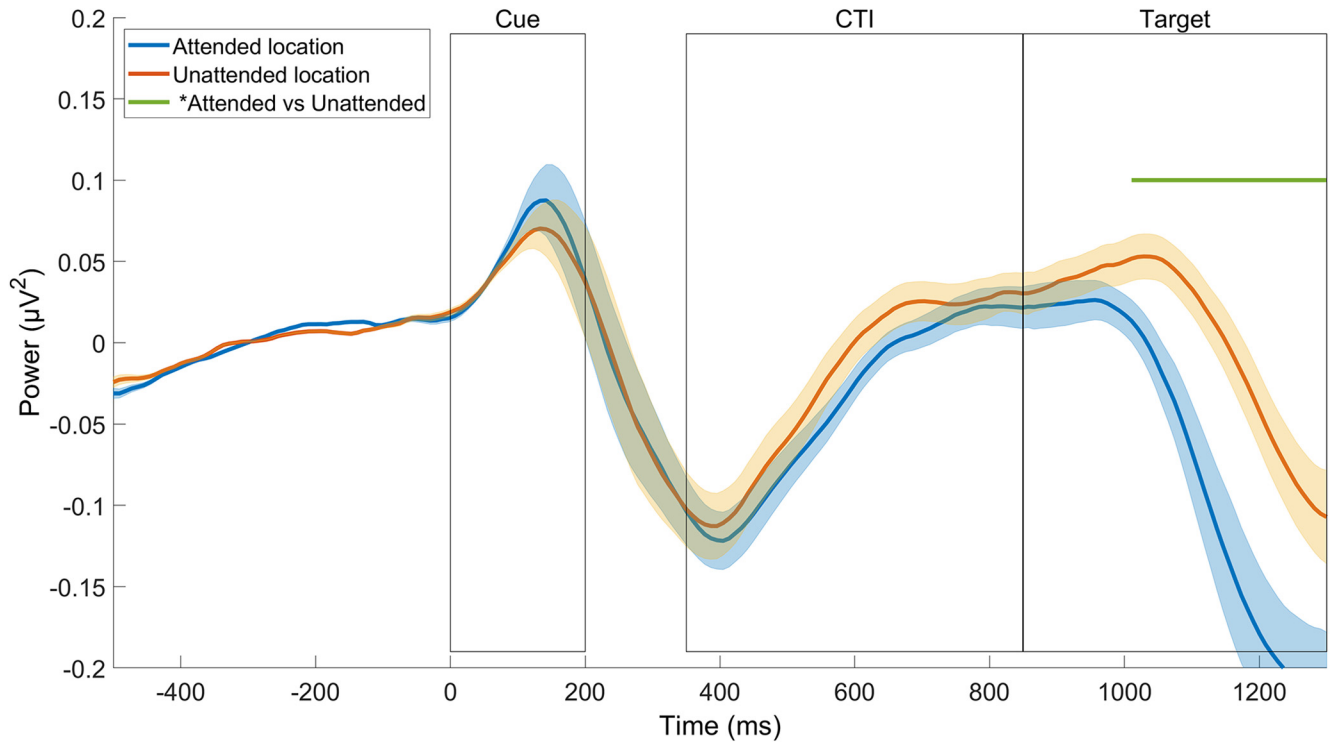


Figure 2. Time course of narrowband α power at a priori-defined ROIs, from horizontal blocks. Boxes indicate cue presentation (onset 0 ms) and periods of the CTI and Target used for stationary frequency analyses (see Figs. 11 and 12). Shaded areas around the data lines represent the SEMs. Horizontal line above the data indicates time points with statistically significant comparisons (second-level statistic on cluster-based permutation analysis, $p \leq 0.01$).

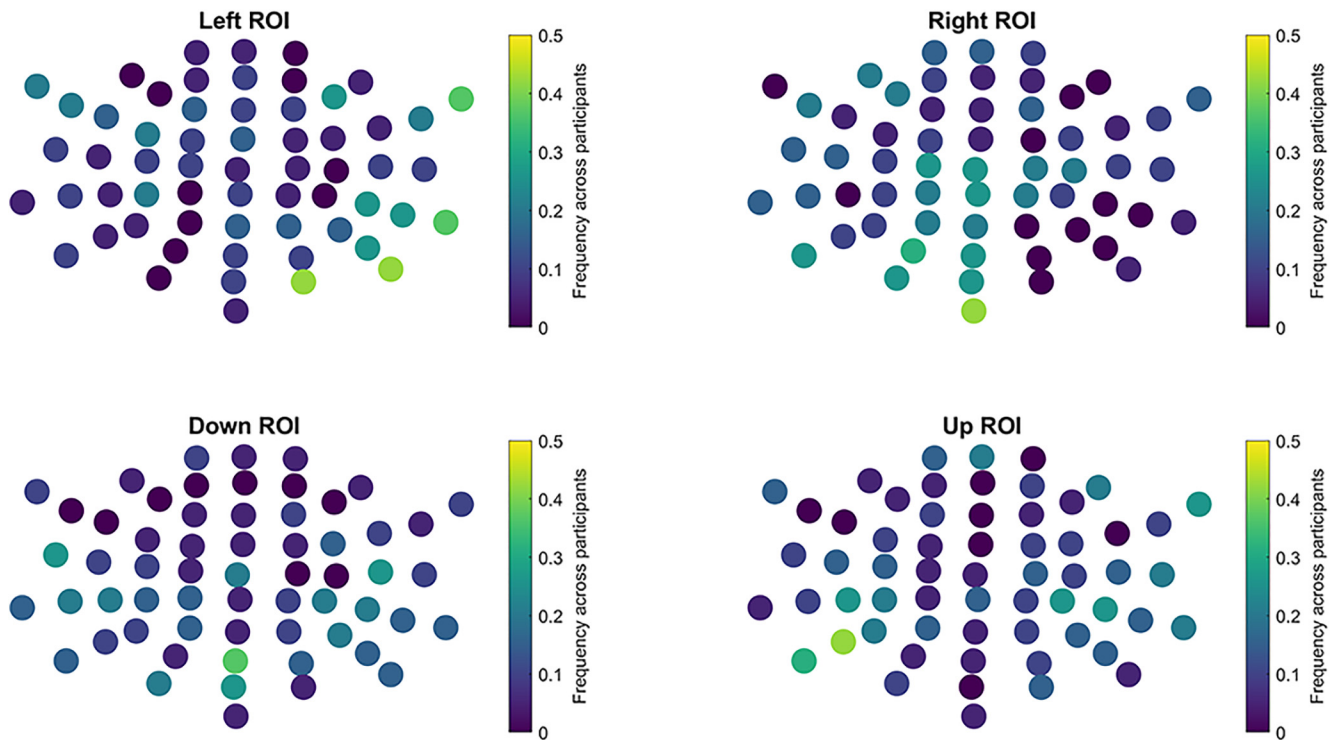


Figure 3. Frequency maps of electrodes selected by multivariate modeling (LASSO for 13/19 participants and mLEM for the remaining ones) of narrowband α power activity during the target-presentation window. The color represents the frequency with which each electrode was selected as a part of that ROI within the sample of subjects.

for selecting the best model parameter, with a 10-fold cross-validation procedure. To avoid bias in the classification due to unbalanced numbers of samples per class, in each run a down-sampling procedure was applied to each of the three nontested position samples to balance the

final number of samples per class (~ 100 tested location trials vs ~ 33 nontested location trials \times three positions).

Across each inner loop iteration, the model that showed the least mean squared error was selected, and electrodes with negative β

coefficients (positive for $1/f$ slope) were selected for the current tested position in the current outer loop iteration. To verify which electrodes were selected consistently across the outer loop iterations, a bootstrap statistical analysis was implemented (Efron, 1992). Specifically, electrodes that were selected with a frequency statistically different from 0 across the outer loop iterations were chosen for the tested location ROI (99% outside the confidence interval estimated from 1000 random samples with replacement).

The LASSO procedure on the narrowband α power data was able to define one ROI for each of the four tested positions in 13 out of 19 subjects, with an average of seven meaningful electrodes per ROI (up $M = 6.79$, $SD = 5.17$; right $M = 7.71$, $SD = 2.93$; down $M = 7.06$, $SD = 3.55$; left $M = 6.88$, $SD = 3.76$; Fig. 3). Across the remaining six participants, LASSO failed to define the up ROI five times, the right ROI two times, the down ROI one time, and the left ROI two times. Correspondingly, the classification procedure on the decomposed α power data was successful for 12 out of 19 subjects, with an average of eight meaningful electrodes per ROI (up $M = 6.19$, $SD = 3.34$; right $M = 9.50$, $SD = 3.61$; down $M = 7.42$, $SD = 4.48$; left $M = 8.47$, $SD = 3.30$; Fig. 4). Across the remaining seven participants, LASSO failed to define the up ROI three times, the right ROI three times, and the left ROI four times. Finally, the classification procedure on the $1/f$ slope data was successful for 12 out of 19 subjects, with an average of 10 meaningful electrodes per ROI (up $M = 8.00$, $SD = 3.92$; right $M = 11.15$, $SD = 4.88$; down $M = 9.89$, $SD = 4.14$; left $M = 10.28$, $SD = 4.20$; Fig. 5). Across the remaining seven participants, LASSO failed to define the up ROI three times, the right ROI six times, and the left ROI one time. For each trial, the narrowband α power data, the decomposed α power data, and the $1/f$ slope data from each ROI were relabeled to correspond to attentional priority status, i.e., attended, unattended or irrelevant. Finally, to simplify the subsequent statistical analysis, activity from the two irrelevant locations, i.e., $+90^\circ$ and -90° from the attended position, was averaged.

mIEM

When the LASSO procedure failed to define all of the four different ROIs, a mIEM was implemented (Sprague and Serences, 2013; Samaha et al., 2016). For each subject, the response at each electrode was modeled as a linear sum of four hypothetical information channels (one per location tested), each corresponding to a δ function centered at its preferred location (i.e., 0° , 90° , 180° , and 270° of polar angle). For all trials except the one held out for cross validation, a general linear model was solved by regressing the EEG activity from the target window (separately for narrowband α power, decomposed α power, and $1/f$ slope) against the basis set of information channels. Next, the resultant matrix containing the mappings of each electrode to the four locations was inverted, and the model tested by feeding it the EEG activity from each of the 60 electrodes from the held-out trial and transforming this into a set of estimated channel responses. This procedure was repeated until every trial served as a test trial in a leave-one-out cross-validation procedure. Finally, for each location, we identified the group of electrodes whose activity was most selective for that location. To select the electrodes most selective for each location, β coefficient matrix values were standardized by subtracting the average across the channels' β values. From the average-corrected β coefficients matrix, the 7, 8, and 10 electrodes with the most negative values (most positive for exponent) were selected for each of the four positions tested, respectively for narrowband α power, for decomposed α power, and for $1/f$ slope. The choice of selecting a number of electrodes equal to the average of the ROIs size found with the LASSO procedure is justified by the assumption that this could be the optimal number of electrodes in this experiment for representing one out of four spatial locations.

Time-frequency series analyses

Evidence for differences between the three attentional priority conditions was assessed statistically using a cluster-based permutation procedure (Maris and Oostenveld, 2007), which was run for each two-conditions comparison: attended versus unattended; attended versus irrelevant; and unattended versus irrelevant. Clusters were defined as

temporally contiguous timepoints in which two experimental conditions showed a significant difference with a first-level-dependent sample t test ($p \leq 0.05$). The second-level statistic was defined as the sum of the t statistics of the timepoints in a cluster, obtained by randomly permuting the data between the two experimental conditions within every subject (1000 permutation with Monte Carlo method). Clusters that showed t values outside the confidence interval were identified as significant ($p \leq 0.01$). Additionally, Bayes factors (BFs) were estimated for each two-conditions comparison, after averaging the data across the significant clusters of timepoints. In instances of nonsignificant two-condition comparisons, the BF was estimated after averaging the data across the smaller significant cluster of timepoints found in the statistical comparisons between the other attentional priority conditions.

Control analysis on stationary frequency activity

Because the FOOOF toolbox (Donoghue et al., 2020b) was originally developed and optimized on stationary frequency activity (Donoghue et al., 2020b), it was important for us to establish the validity of using the method on time-frequency series data, as we intended to do for this experiment. To do this, decomposed α power and $1/f$ slope were derived with the FOOOF algorithm from a Welch's method spectral distribution (Welch, 1967) as a control analysis. Specifically, a Welch's method frequency decomposition (1–50 Hz, 0.25 Hz frequencies bins) was run separately on each electrode, each trial, for each subject, across three different time intervals: a baseline interval between -500 and 0 ms, a CTI interval between 350 and 850 ms, and a target presentation interval between 850 and 1350 ms. Similarly to the main analysis, the FOOOF algorithm (Donoghue et al., 2020b) estimated peak α power and exponent values, separately for each electrode, each trial, each subject and each time interval. Finally, the peak α power and exponent values were averaged across the electrodes of each ROI and relabeled accordingly to their attentional priority status, i.e., attended, unattended and irrelevant, and activity from the two irrelevant locations, i.e., $+90^\circ$ and -90° from the attended position, were averaged.

Eye-tracking recording and analysis

Eye position across x - and y -axes was recorded monocularly from the right eye with an infrared-based eye tracker with sampling rate of 1000 Hz and a spatial resolution of 0.01° (EyeLink 1000; SR Research). Movements of the head were limited by a chin rest. Before each experimental block, a standard nine-point-grid calibration was performed, to allow for conversion from raw eye position to gaze position. During the calibration procedure, subjects fixated white dots (1°), serially presented at different locations on the screen, corresponding to a 3×3 array centered on the center of the screen, starting at the upper-left and proceeding in a left-to-right and up-to-down order. Immediately after each calibration procedure, a validation procedure was run, to verify the accuracy of the calibration. During validation dots were presented in a random order; x - and y -eye gaze data were converted from screen pixels to degree of angle. Blink intervals were identified with a blink detection algorithm and verified by a rater. In order to carry out analyses on microsaccades, blink intervals were removed from the data, along with samples from 200 ms preceding to 200 ms following each blink. Blink-free gaze position data were then segmented into epochs from -1 to 1999 ms relative to cue onset. Microsaccades were identified by an expert rater and validated by a secondary rater, blind to the purpose of the study, by visually inspecting the segmented x - and y -gaze data. Eye-movement events larger than 1 DVA and outside the CTI were excluded from the analysis. Time, amplitude, and direction of each microsaccade was recorded. In order to whether the direction of a microsaccade was toward the attended location, microsaccade directions were rotated to align the different to-be-attended trial directions on a common attended direction, set to 0° .

Results

Behavioral performance

Collapsed across axis (horizontal, vertical), mean accuracy was higher for validly than invalidly cued trials [72% correct

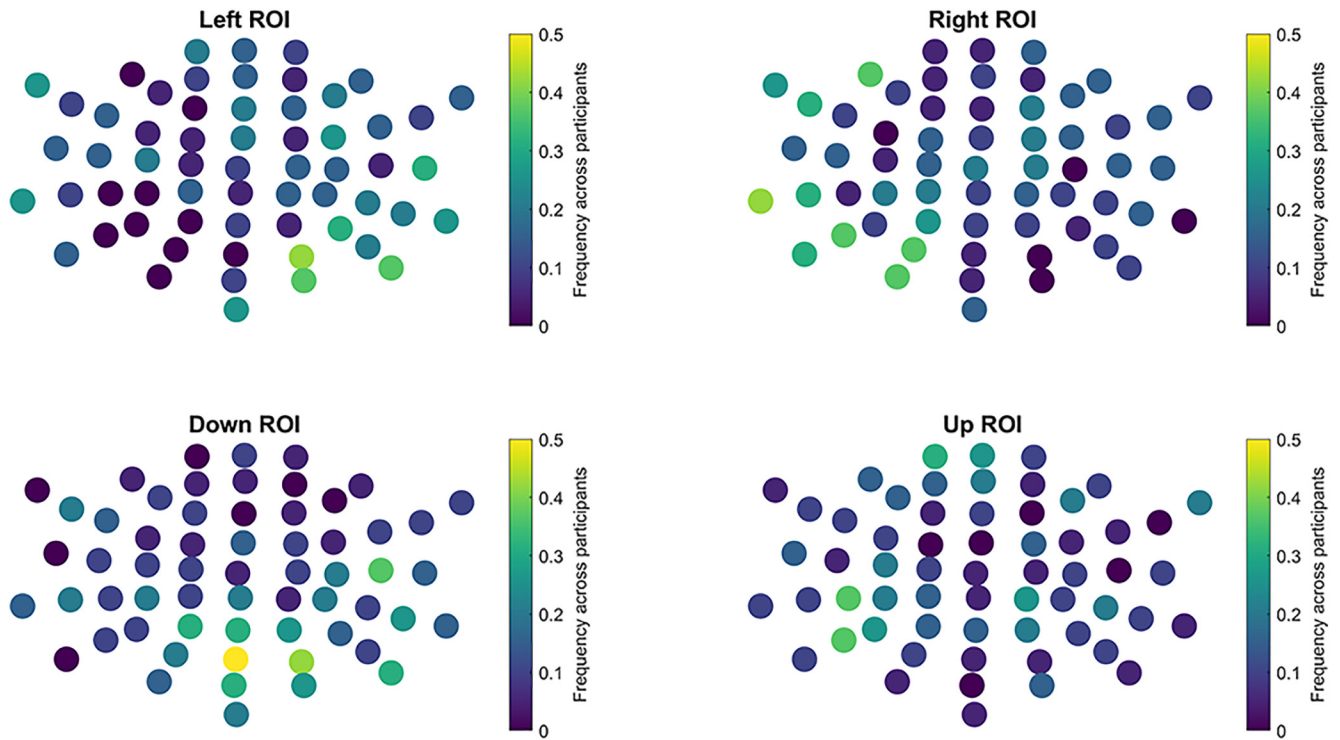


Figure 4. Frequency maps of electrodes selected by multivariate modeling (LASSO for 12/19 participants and mIEM for the remaining ones) of the decomposed α power component of the EEG (after decomposition) during the target-presentation window. The color represents the frequency with which each electrode was selected as a part of that ROI within the sample of subjects.

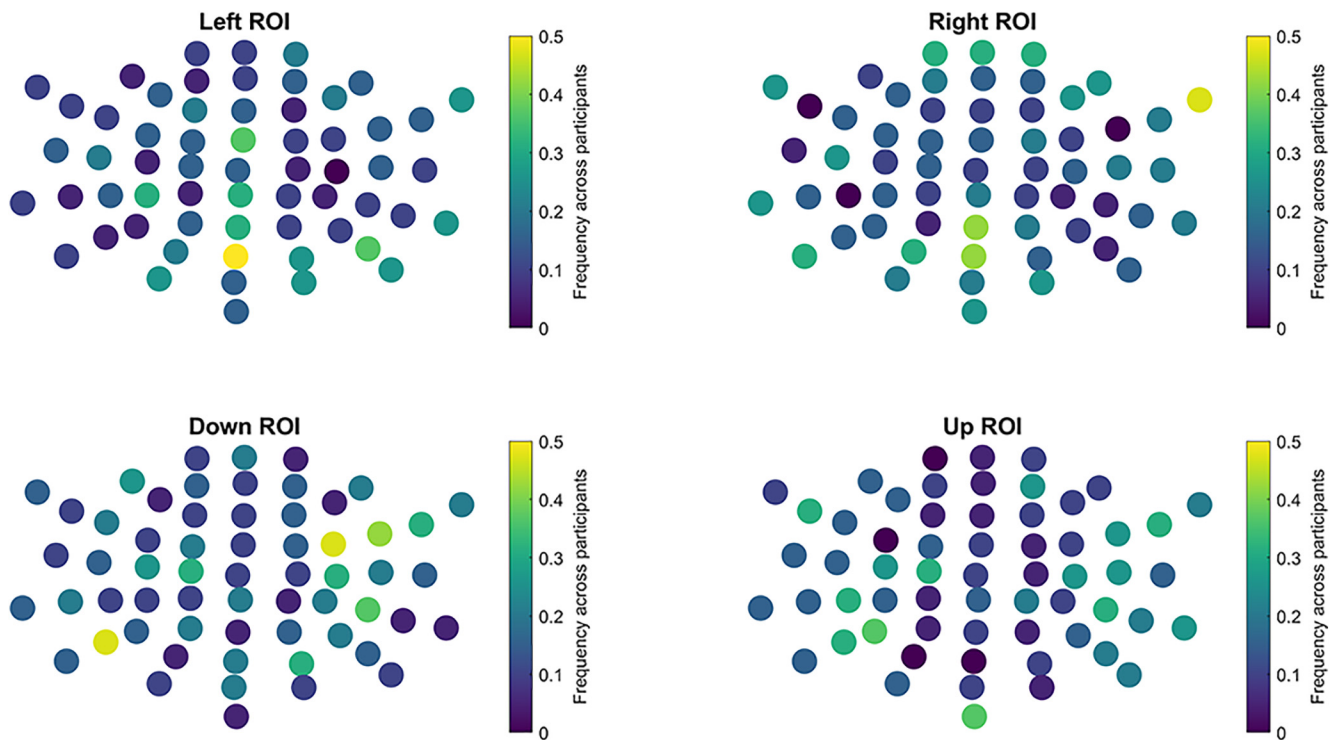


Figure 5. Frequency maps of electrodes selected by multivariate modeling (LASSO for 12/19 participants and mIEM for the remaining ones) of the $1/f$ slope component of the EEG (after decomposition) during the target-presentation window. The color represents the frequency with which each electrode was selected as a part of that ROI within the sample of subjects.

(SD = 10] vs 67% (SD = 9), $d = 0.53$], with similar values for horizontal trials [72% correct (11) vs 66% (12), $d = 0.52$] and vertical trials [71% correct (10) vs 67% (9), $d = 0.42$]. ANOVA with within-subject factors of VALIDITY (validly vs invalidly

cued trials) and AXIS (horizontal vs vertical) confirmed a main effect of VALIDITY ($F_{(1,18)} = 8.85, p < 0.01$), no main effect of AXIS ($F_{(1,18)} = 0.00, n.s.$), and no interaction ($F_{(1,18)} = 0.59, n.s.$). Mean RTs followed a pattern consistent with accuracy:

shorter for valid [1004 ms (309)] than invalid [1070 ms (296), $d = 0.22$], with similar values for horizontal trials [1020 ms (331) vs 1081 ms (294), $d = 0.19$] and vertical trials [988 ms (290) vs 1059 ms (309), $d = 0.24$]. ANOVA revealed a main effect of VALIDITY ($F_{(1,18)} = 4.44$, $p = 0.04$), no main effect of AXIS ($F_{(1,18)} = 1.77$, n.s.), and no interaction effect ($F_{(1,18)} = 0.22$, n.s.). Visibility ratings followed a pattern consistent with the objective measures, with higher mean ratings for valid [2.27 (0.53)] than invalid [2.04 (0.52), $d = 0.44$] trials, and again with similar values for horizontal trials [2.28 (0.53) vs 2.07 (0.51), $d = 0.40$] and vertical trials [2.27 (0.55) vs 2.00 (0.54), $d = 0.50$], ANOVA again revealing a main effect of VALIDITY ($F_{(1,18)} = 6.59$, $p = 0.02$), no effect of AXIS ($F_{(1,18)} = 1.53$, n.s.), and no interaction ($F_{(1,18)} = 1.93$, n.s.).

The mean percentage of trials in which one or more microsaccade was detected was 46%: right cued [45% (20)], down cued [43% (16)], left cued [47% (18)], up cued [48% (18)], values that did not differ ($F_{(3,45)} = 2.05$, n.s.), and they occurred an average of 405 ms after the cue presentation. A second microsaccade was detected on 41% of these trials: right cued [39% (22)], down cued [41% (19)], left cued [43% (21)], up cued [39% (22)], values that did not differ ($F_{(3,45)} = 0.55$, n.s.), they occurred an average of 573 ms after cue presentation, and 63% of them were a return to fixation. In order to test whether microsaccades executed during the CTI were biased toward the attended location, violation of a uniform distribution of microsaccades around the attended location (0 DVA) was verified with a V test (Zar, 1999), run with the CircStat toolbox (Berens, 2009) on MATLAB (2020b, The MathWorks). The distribution of the direction of microsaccades during the CTI was significantly nonuniform, and biased toward the attended position ($M = +5.62^\circ$, $AD = 0.94^\circ$; $V_{(1,18)} = 6.60$, $p = 0.01$, $d = 5.98$). To summarize, microsaccades were biased toward the attended location from ~ 400 ms after the spatial cue presentation, suggesting the influence of spatial expectations also on the control of eye-movements.

Narrowband α power

Narrowband α power recorded from the electrodes representing the attended location was significantly lower compared with electrodes representing the unattended location, starting from 386 ms after cue presentation and lasting until the end of the trial ($p > 0.001$, $BF_{10} > 10$), and it differed from the electrodes representing the irrelevant locations starting from 84 ms before cue presentation and lasting until the end of the trial ($p > 0.001$, $BF_{10} > 10$). Of primary importance for the question that we set out to address, narrowband α power showed moderate evidence in favor of an absence of a difference in the activity between electrodes representing the unattended and the irrelevant locations at any point during the trial ($BF_{10} = 0.24$; Fig. 6).

Following the logic of our design, the moderate evidence for an absence of a difference between ROIs representing unattended and irrelevant locations is consistent with secondary-consequence accounts of attention-related α dynamics: when attention selects a location, the physiological state of all other locations returns to a common baseline level.

Decomposed EEG signals

The idea motivating the decomposition of the EEG into periodic and aperiodic components is that the conventional method of bandpass filtering leaves uncertain whether attention-related effects like those illustrated in Figure 6A are because of effects of attention on true oscillations in the 8- to 14-Hz range, on

aperiodic components that also influence this range, or on some mixture of the two. To address these questions comprehensively, we examined the dynamics of the decomposed α and 1/f slope signals in each of two sets of ROIs: the ROIs generated with narrowband α data (Fig. 3) and the ROIs generated with the decomposed α and 1/f slope signals, respectively (Figs. 4, 5). The reason for doing so in the narrowband- α ROIs is to assess the extent to which the pattern observed in Figure 6A (which broadly replicates a well-established finding in the literature for attended vs unattended electrodes), is because of “true” α band oscillations or to aperiodic elements in the narrowband signal. Additionally, however, it is important to note that the narrowband- α ROIs may not be selective for up, right, down, and left for either the decomposed α or the 1/f slope signals. Stated another way, the topography of retinotopy for either of these two putatively independent generators may be different that it is for the scalp-level EEG signal that is a mixture of the two. Thus, a more valid way to assess the effects of spatial cueing on decomposed α is to identify electrodes that are selective for the representation of these four locations by decomposed α , and the same is true for 1/f slope.

Decomposed α power at ROIs spatially selective for narrowband α

In the ROIs identified by regressing target-related narrowband α power, decomposed α power discriminated between attended and both unattended and irrelevant locations, but only during target presentation (Fig. 7A). Specifically, decomposed α power recorded from the electrodes representing the attended location was significantly lower compared with electrodes representing the unattended location, starting from 929 ms after cue presentation and lasting until the end of the trial ($p < 0.001$, $BF_{10} > 10$). Furthermore, the decomposed α power recorded from the attended location was also significantly lower compared with electrodes representing the task-irrelevant, starting from 812 ms and lasting until the end of the trial ($p < 0.001$, $BF_{10} > 10$). Finally, no significant difference was found between unattended and irrelevant locations across the entire duration of the trial (all $p > 0.01$, $BF_{10} = 0.41$). Overall, decomposed α power at ROIs spatially selective for narrowband α failed to show differential modulation of any of the ROIs during the CTI, suggesting a lack of correspondence between narrowband and decomposed α power distribution across the scalp.

Decomposed α power at ROIs spatially selective for decomposed α power

In the signal-selective ROI, decomposed α power only discriminated between the three attentional priority states during target presentation (Fig. 8A). As was the case with narrowband α , the divergence of decomposed α power corresponding to the attended versus the irrelevant location began earlier (694 ms after cue presentation; $p < 0.001$, $BF_{10} > 10$) than the divergence of attended to unattended (902 ms after cue presentation; $p < 0.001$, $BF_{10} > 10$). Unlike narrowband α , however, decomposed α power corresponding to the unattended location did eventually diverge from decomposed α power corresponding to the irrelevant location, taking on a higher value starting from 1083 ms after cue presentation ($p < 0.001$, $BF_{10} > 10$). Note that because all of these effects occurred shortly before, or after, the onset of the target, it is unlikely that they reflect an important contribution to a cue-triggered anticipatory shift of spatial attention.

1/f slope at ROIs spatially selective for narrowband α

In the ROIs identified by regressing target related narrowband α power, 1/f slope discriminated between attended and both

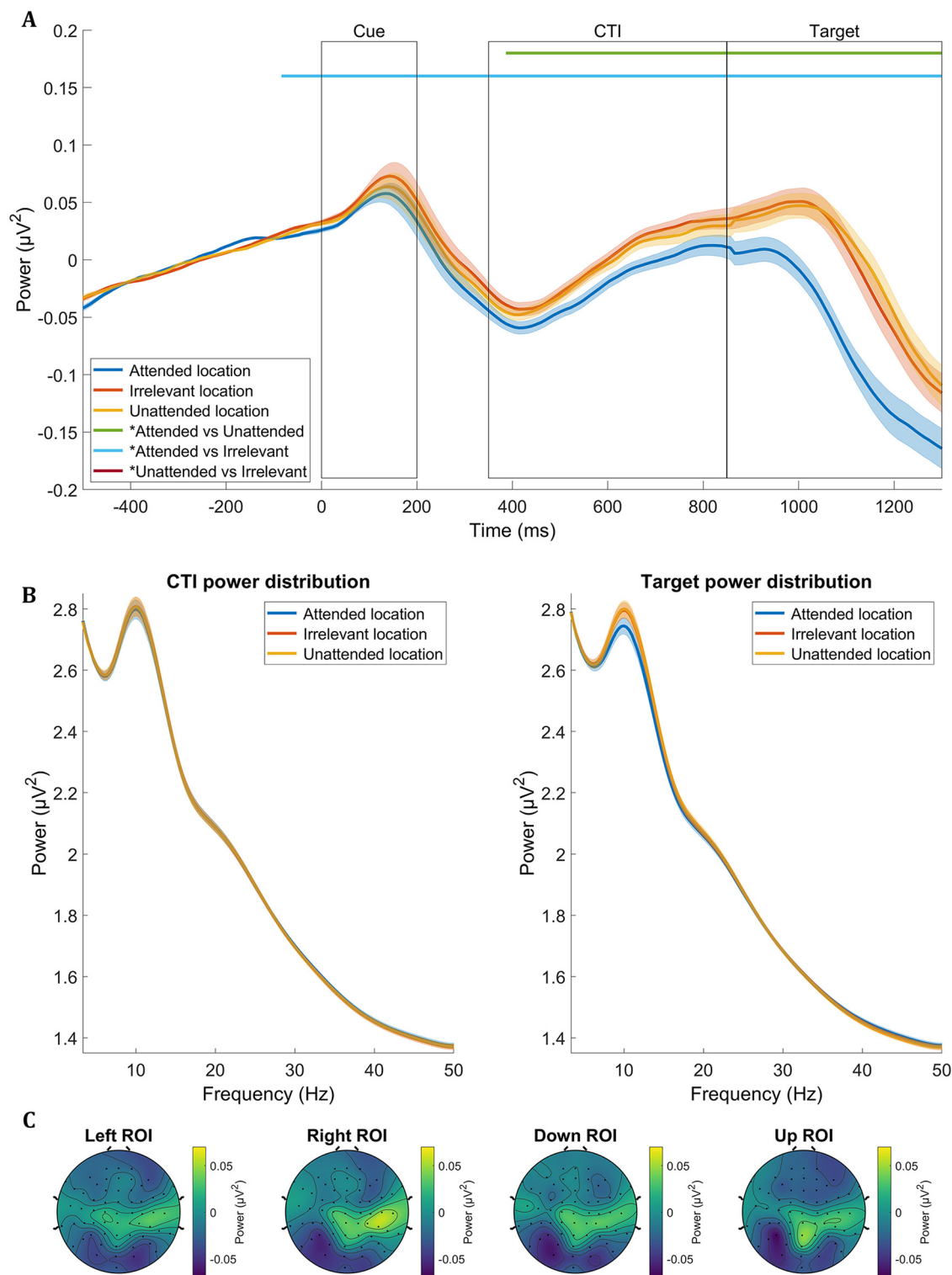


Figure 6. *A*, Time course of narrowband α power across ROIs derived from multivariate analyses of narrowband α power data (Fig. 3). Shaded areas around the data lines represent the SEMs. Horizontal lines above the data indicate time points with statistically significant comparisons (second-level statistic on cluster-based permutation analysis, $p \leq 0.01$). *B*, Spectral distributions across ROIs derived from multivariate analyses of narrowband α power data averaged across CTI (box in panel A encompassing 350–850 ms) and target presentation (box in panel A encompassing 850–1300 ms) time windows. Shaded areas around the data lines represents the SEMs. *C*, Topographies of the narrowband α power averaged across the CTI time window (350–850 ms) for each cued location.

unattended and irrelevant locations, but only during target presentation (Fig. 9). Specifically, 1/f slope from the attended location was significantly lower compared with electrodes representing the unattended location, starting from 1002 to 1191 ms ($p < 0.001$, $\text{BF}_{10} > 10$), and similarly was significantly

lower compared with irrelevant location, starting from 1002 to 1173 ms ($p < 0.001$, $\text{BF}_{10} > 10$). Finally, no significant difference was found between unattended and irrelevant locations across all the trial duration (all $p > 0.01$, $\text{BF}_{10} = 0.24$). Thus, in the same way as for the decomposed α power, 1/f slope at

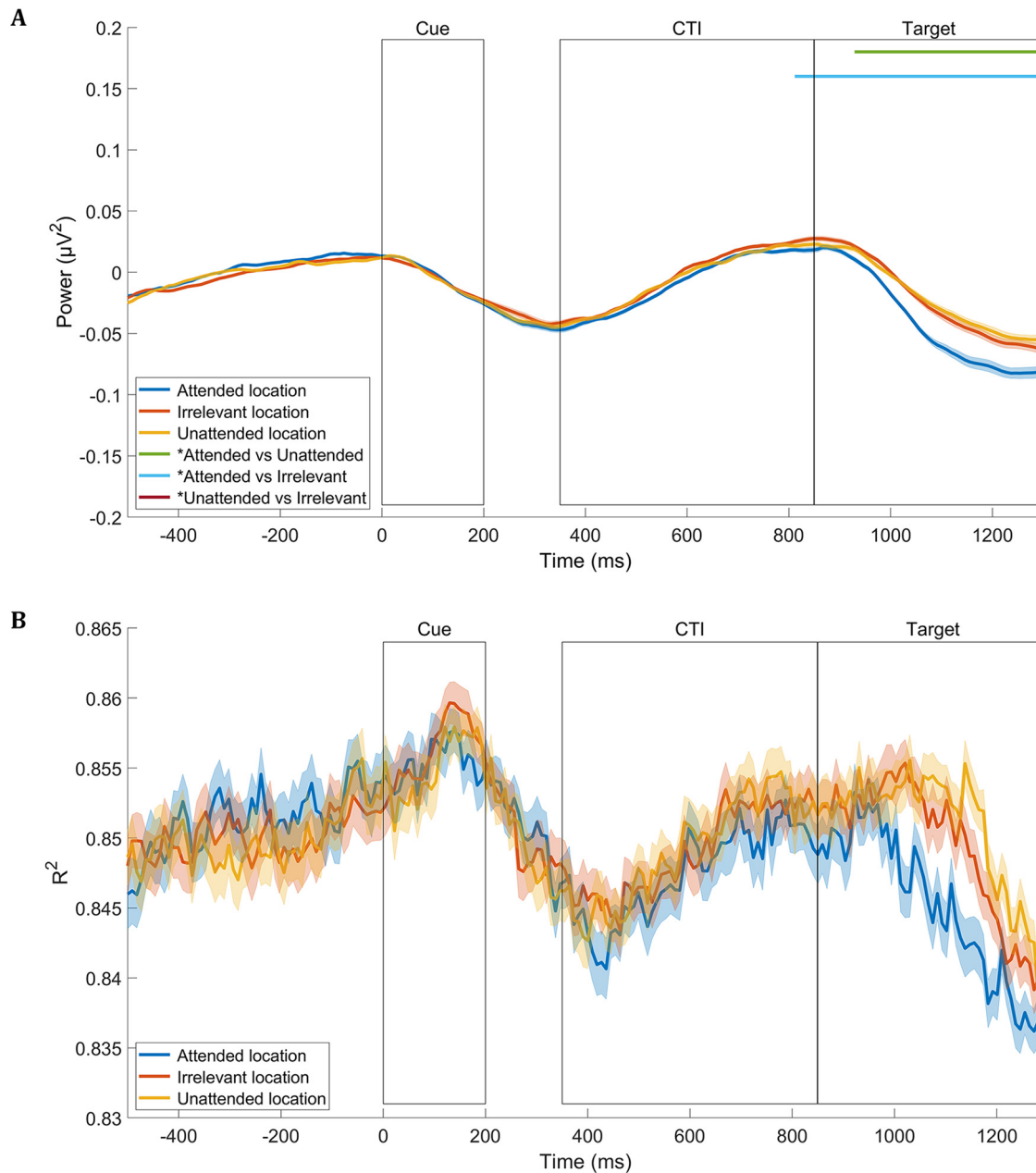


Figure 7. Time course of decomposed α power (A) and R^2 from F00F parametrization (B) across ROIs derived from multivariate analyses of narrowband α power (Fig. 3). Shaded areas around the data lines represent the SEMs. Horizontal lines above the decomposed α power data indicate time points with statistically significant comparisons (second-level statistic on cluster-based permutation analysis, $p \leq 0.01$).

ROIs spatially selective for narrowband α failed to show a modulation of any of the ROIs during the CTI, suggesting a lack of correspondence between narrowband and $1/f$ slope distribution across the scalp.

1/f slope at ROIs spatially selective for 1/f slope

In a pattern markedly different from narrowband α and decomposed α , $1/f$ slope differed at the irrelevant versus unattended ROI during the pretrial ITI and for the entirety of the trial ($p < 0.001$, $\text{BF}_{10} > 10$), suggesting that $1/f$ slope was tonically elevated at irrelevant ROIs for the entirety of the block. (Recall that, because the factor AXIS was blocked, electrodes corresponding to an irrelevant location retained this status for the duration of each block, e.g., during a block in which either “left” or “right” could be cued, “up” and “down” were never cued.) $1/f$

slope also differed between irrelevant and attended ROIs during the pretrial ITI and for the entirety of the trial ($p < 0.001$, $\text{BF}_{10} > 10$). $1/f$ slope did not differ between attended and unattended ROIs until a window beginning after target onset (from 884 to 1255 ms after cue presentation; $p < 0.001$, $\text{BF}_{10} > 10$), during which $1/f$ slope was greater at the unattended ROI (Fig. 10A). From a physiological perspective, this result suggests that locations that are potential targets of selection (i.e., attended or unattended) may differ from locations that are known to be task-irrelevant in that the excitation-inhibition (E:I) balance in the former is tonically elevated. From an interpretational perspective, this dissociation of irrelevant from unattended suggests that the null findings with the narrowband α and decomposed α signals can, indeed, be interpreted as evidence that attention-related increases in α band power do not reflect an active-suppression

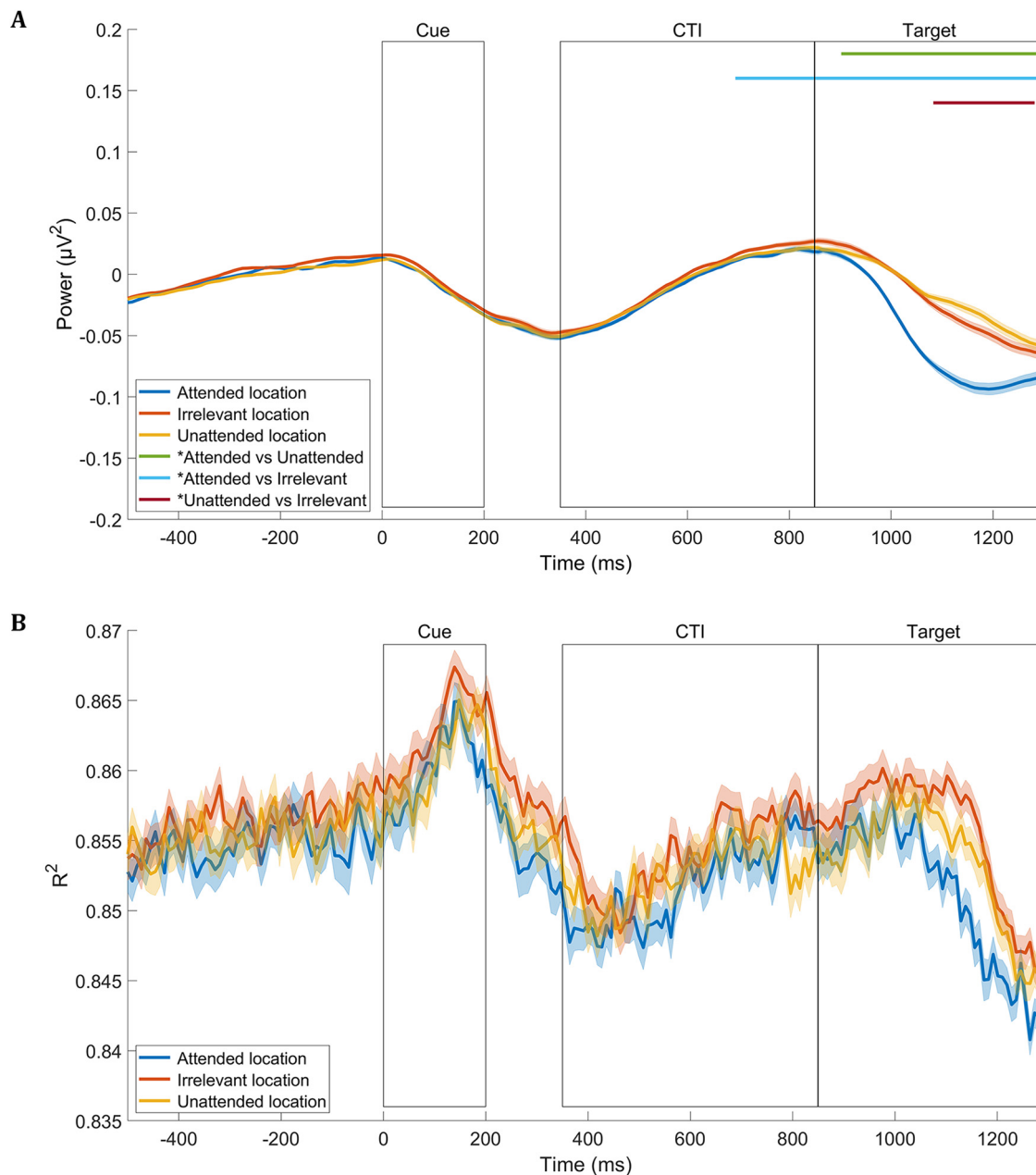


Figure 8. Time course of decomposed α power (**A**) and R^2 from F00F parametrization (**B**) across ROIs derived from multivariate analyses of decomposed α power (Fig. 4). Shaded areas around the data lines represent the SEMs. Horizontal lines above the decomposed α power data indicate time points with statistically significant comparisons (second-level statistic on cluster-based permutation analysis, $p \leq 0.01$).

mechanism, but may instead simply be a consequence of the withdrawal of attention from the unattended region.

Control frequency decomposition

Possible differences between the three attentional priority conditions across the three time intervals were statistically assessed with repeated-measures ANOVAs: one for decomposed α power at ROIs spatially selective for decomposed α power (Fig. 4), and one for $1/f$ slope at ROIs spatially selective for $1/f$ slope (Fig. 5). Each ANOVA had TIME (baseline vs CTI versus target presentation time intervals) and PRIORITY (attended vs unattended vs irrelevant locations) as within-subject factors. All *post hoc* comparisons were conducted using the Newman–Keuls test. These statistical analyses were performed using STATISTICA (version 12.0; StatSoft). In the same way as the statistical analysis on time-

frequency data, BFs were estimated for each two-conditions comparison.

The ANOVA run for decomposed α power at ROIs spatially selective for decomposed α power (Fig. 11A) revealed a significant TIME \times PRIORITY interaction ($F_{(4,72)} = 52.30$, $p < 0.01$). Specifically, for the CTI time interval, the attended ROI [$M = 6.16 \mu\text{V}^2$ (0.24)] showed significantly lower decomposed α power compared with both the irrelevant [$M = 6.20 \mu\text{V}^2$ (0.24), $p = 0.04$, $d = 0.17$, $\text{BF}_{10} = 5.88$] and unattended [$M = 6.19 \mu\text{V}^2$ (0.24), $p = 0.04$, $d = 0.13$, $\text{BF}_{10} = 3.12$] ROIs. And of particular importance for our question of principal interest, decomposed α power showed moderate evidence in favor of an absence of a difference in the activity between electrodes representing the unattended and the irrelevant locations during the CTI ($p = 0.82$, $\text{BF}_{10} = 0.24$). This result replicates and corroborates the evidence

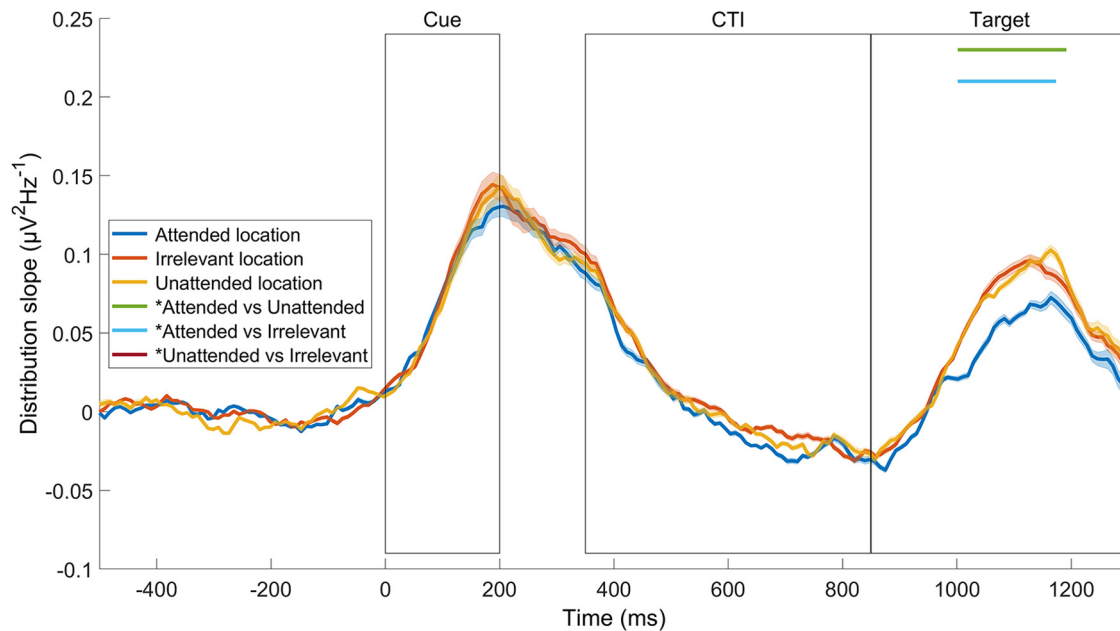


Figure 9. Time course of $1/f$ slope across ROIs derived from multivariate analyses of narrowband α power. Shaded areas around the data lines represent the SEMs. Horizontal lines above the data indicate time points with statistically significant comparisons (second-level statistic on cluster-based permutation analysis, $p \leq 0.01$). (Note that higher values correspond to steeper slope.)

for an absence of difference between unattended and irrelevant location found for narrowband α power in the time–frequency analysis.

Moreover, for the target presentation time interval, the attended ROI [$M = 5.83 \mu\text{V}^2$ (0.19)] showed a significantly lower decomposed α power compared with both the irrelevant [$M = 6.02 \mu\text{V}^2$ (0.20), $p < 0.01$, $d = 0.97$, $\text{BF}_{10} > 10$] and unattended [$M = 6.05 \mu\text{V}^2$ (0.20), $p < 0.01$, $d = 1.13$, $\text{BF}_{10} > 10$] ROIs, and the irrelevant ROI showed a significantly lower decomposed α power compared with the unattended ($p = 0.02$, $d = 0.15$, $\text{BF}_{10} = 2.22$) ROI. Finally, no significant *post hoc* tests were found to be significant for the baseline time interval (all p s > 0.11). Additionally, significant main effects of both TIME ($F_{(2,36)} = 4.97$, $p = 0.01$) and PRIORITY ($F_{(2,36)} = 40.7$, $p < 0.01$) were found, described by significantly lower decomposed α power during target presentation [$M = 5.96 \mu\text{V}^2$ (0.20)] compared with both baseline [$M = 6.15 \mu\text{V}^2$ (0.25), $p = 0.02$, $d = 0.84$, $\text{BF}_{10} = 1.69$] and CTI [$M = 6.18 \mu\text{V}^2$ (0.24), $p = 0.02$, $d = 0.96$, $\text{BF}_{10} = 4.32$] time intervals, and by lower decomposed α power in the attended ROI [$M = 6.05 \mu\text{V}^2$ (0.23)] compared with both irrelevant [$M = 6.12 \mu\text{V}^2$ (0.23), $p < 0.01$, $d = 0.30$, $\text{BF}_{10} > 10$] and unattended ROIs [$M = 6.13 \mu\text{V}^2$ (0.23), $p < 0.01$, $d = 0.35$, $\text{BF}_{10} > 10$]. Overall, decomposed α power, estimated on stationary frequency activity, showed a similar modulation of ROIs representing unattended and irrelevant locations, also suggesting that spatial expectations modulations on true periodic α power do not discriminate between unattended and irrelevant locations.

The ANOVA run for the $1/f$ slope at ROIs spatially selective for $1/f$ slope (Fig. 12A) revealed a significant TIME \times PRIORITY interaction ($F_{(4,72)} = 23.67$, $p < 0.01$). Specifically, for the baseline time interval, the irrelevant ROI [$M = 5.84 \mu\text{V}^2\text{Hz}^{-1}$ (0.20)] showed a significantly higher $1/f$ slope compared with both the attended [$M = 5.69 \mu\text{V}^2\text{Hz}^{-1}$ (0.20), $p < 0.01$, $d = 0.75$, $\text{BF}_{10} > 10$] and unattended [$M = 5.71 \mu\text{V}^2\text{Hz}^{-1}$ (0.20), $p < 0.01$, $d = 0.65$, $\text{BF}_{10} > 10$] ROIs, whereas no significant difference was found between attended and

unattended ROIs ($p = 0.37$, $\text{BF}_{10} = 0.36$). Similarly, for the CTI time interval, the irrelevant ROI [$M = 5.86 \mu\text{V}^2\text{Hz}^{-1}$ (0.20)] showed a significantly higher $1/f$ slope compared with both the attended [$M = 5.75 \mu\text{V}^2\text{Hz}^{-1}$ (0.20), $p < 0.01$, $d = 0.55$, $\text{BF}_{10} > 10$] and unattended [$M = 5.74 \mu\text{V}^2\text{Hz}^{-1}$ (0.20), $p < 0.01$, $d = 0.60$, $\text{BF}_{10} > 10$] ROIs, whereas no significant difference was found between attended and unattended ROIs ($p = 0.89$, $\text{BF}_{10} = 0.24$). Finally, for the target presentation time interval, the irrelevant ROI [$M = 6.18 \mu\text{V}^2\text{Hz}^{-1}$ (0.20)] showed a significantly higher $1/f$ slope compared with both the attended [$M = 5.90 \mu\text{V}^2\text{Hz}^{-1}$ (0.20), $p < 0.01$, $d = 1.4$, $\text{BF}_{10} > 10$] and unattended [$M = 6.00 \mu\text{V}^2\text{Hz}^{-1}$ (0.20), $p < 0.01$, $d = 0.90$, $\text{BF}_{10} > 10$] ROIs, and the unattended ROI showed a significantly higher $1/f$ slope compared with the attended ($p = 0.02$, $d = 0.5$, $\text{BF}_{10} > 10$) ROI. Additionally, significant main effects of both TIME ($F_{(2,36)} = 33.7$, $p > 0.01$) and PRIORITY ($F_{(2,36)} = 45.9$, $p < 0.01$) were found, corresponding to a significantly higher $1/f$ slope during target presentation [$M = 6.02 \mu\text{V}^2\text{Hz}^{-1}$ (0.20)] compared with both baseline [$M = 5.75 \mu\text{V}^2\text{Hz}^{-1}$ (0.20), $p < 0.01$, $d = 1.35$, $\text{BF}_{10} > 10$] and CTI [$M = 5.78 \mu\text{V}^2\text{Hz}^{-1}$ (0.20), $p < 0.01$, $d = 1.20$, $\text{BF}_{10} > 10$] time intervals, and by a higher $1/f$ slope in the irrelevant ROI [$M = 5.96 \mu\text{V}^2\text{Hz}^{-1}$ (0.20)] compared with both attended [$M = 5.78 \mu\text{V}^2\text{Hz}^{-1}$ (0.20), $p < 0.01$, $d = 0.9$, $\text{BF}_{10} > 10$] and unattended ROIs [$M = 5.82 \mu\text{V}^2\text{Hz}^{-1}$ (0.20), $p < 0.01$, $d = 0.70$, $\text{BF}_{10} > 10$]. Overall, $1/f$ slope, estimated on stationary frequency activity, was tonically higher in the ROI representing irrelevant locations compared with both attended and unattended locations across the duration of the trial as well as the ITI time interval, also suggesting that expectations about the spatial configuration of the current block modulate the aperiodic component of the spectral distribution in a tonic manner.

Discussion

In this experiment, we blocked trials such that, in any given block, targets would only appear in two of four possible

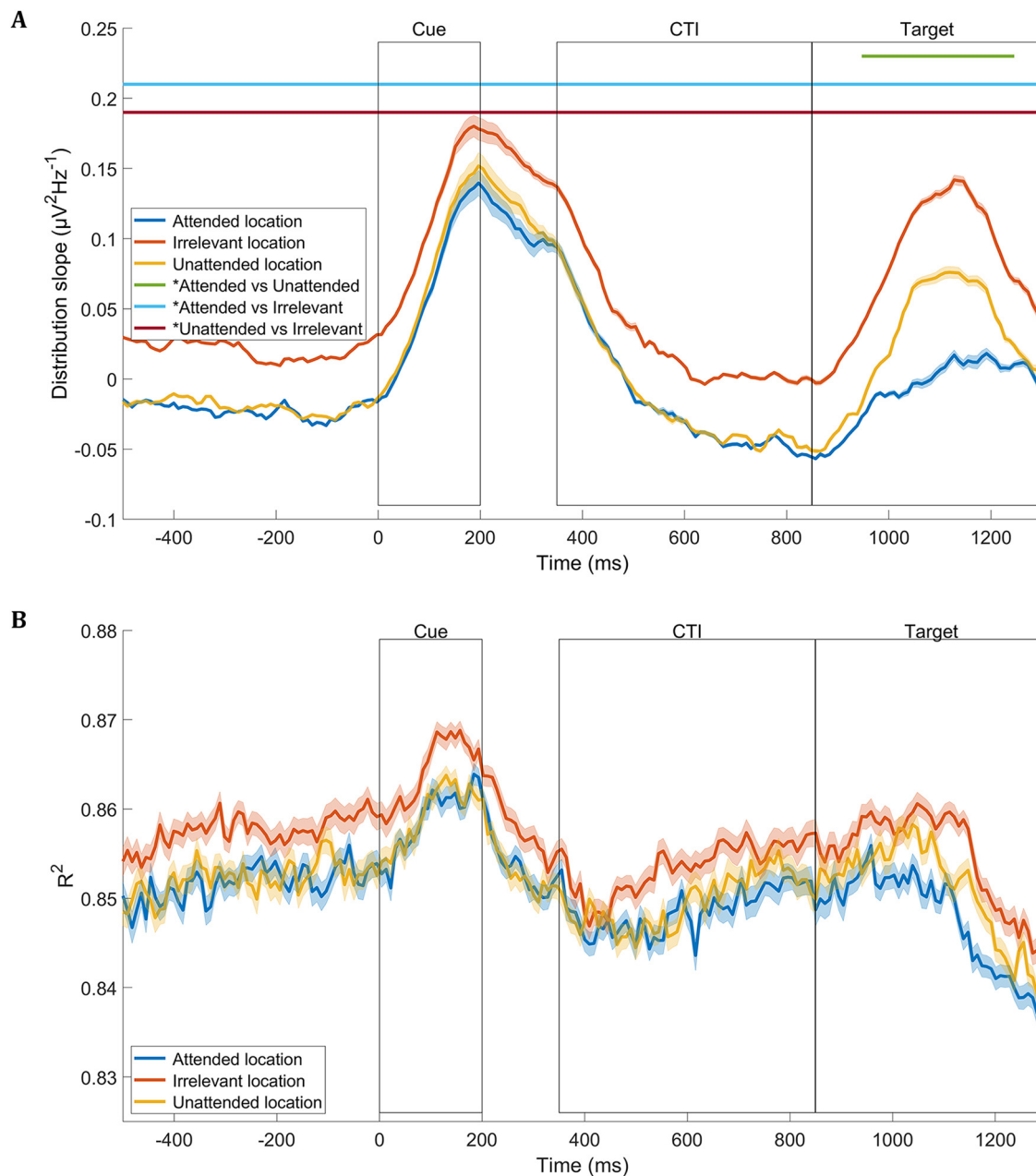


Figure 10. Time course of $1/f$ slope (**A**) and R^2 from FOOOF parametrization (**B**) across ROIs derived from multivariate analyses of $1/f$ slope (Fig. 5). Shaded areas around the data lines represent the SEMs. Horizontal lines above the $1/f$ slope data indicate time points with statistically significant comparisons (second-level statistic on cluster-based permutation analysis, $p \leq 0.01$). (Note that in **A**, higher values correspond to steeper slope.)

locations, thereby rendering the other two locations irrelevant during that block. Behaviorally, the spatial information conveyed by the symbolic cue influenced performance in ways that are well established in the literature: improved discrimination on validly cued trials, and a biased pattern of microsaccades during the CTI. Starting with the narrowband α signal (i.e., the signal comparable to that used in the vast majority of studies of spatial attention to date), our results replicated the canonical pattern of the cue-triggered dissociation of α power at attended versus unattended locations. Of principal theoretical interest, they also showed that the dynamics of α power at irrelevant locations very closely matched those of α power at unattended locations. This finding is difficult to reconcile with interpretations of α as a mechanism for the implementation of attention control (Kelly et al., 2006; Jensen and Mazaheri, 2010; Sadaghiani and Kleinschmidt, 2016), and instead

offers support for the possibility that attention-related changes in α power may be consequences of some other factors (Antonov et al., 2020). For example, if selection of the attended location is accomplished via increased input (via spiking) from cortical circuits in the dorsal attention network (DAN; Corbetta and Shulman, 2002), this increased input may cause a decrease in α power; concomitantly, a decrease in top-down input at nonselected areas, combined with lateral inhibition from the selected location, would result in an increase in α power. Furthermore, the facts that $1/f$ slope did not differ between attended and unattended locations during the CTI (although it did differ for the irrelevant location), and that this effect persisted throughout the block, including during the ITI, suggests that physiological state (perhaps E:I balance) is modified at locations where selection is predicted to occur.

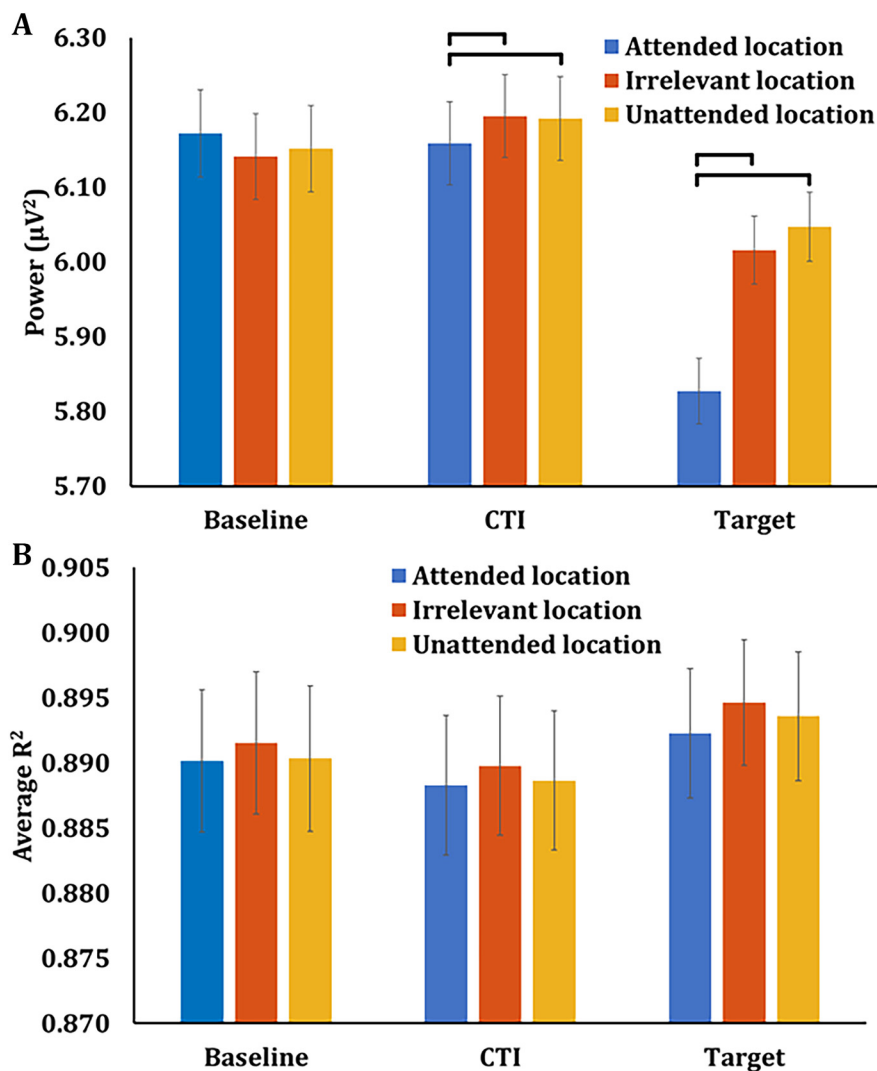


Figure 11. Decomposed α power (A) and R^2 (B) from FOOOF parametrization across baseline (−500–0 ms), CTI (350–850 ms), and target presentation (850–1350 ms) epochs, from ROIs derived from multivariate analyses of decomposed α power (Fig. 4). Black lines indicate statistically significant comparisons (Newman–Keuls, $p \leq 0.05$).

A convention for EEG studies of Posner-style cueing tasks is to cue targets to the right or left of fixation, then label signals from a predefined set of electrodes contralateral to the cue as “attended” and from a predefined set of electrodes ipsilateral to the cue as “unattended.” One limitation of this approach is that it does not allow for the distinction between “unattended” and “irrelevant.” This is important because if the increase in α power at unattended electrodes is truly a mechanism deployed to inhibit processing at the unattended location, one should expect this signal to be retinotopically focused. [To be sure, the spatial resolution of EEG is coarse; nonetheless, to be logically consistent, if one is willing to interpret relatively focal patterns of α desynchronization as indicative of the focus of spatial attention (cf. Samaha et al., 2016, their Fig. 2), one should also expect that “focal suppression” would produce comparably focal patterns of α synchronization.] To be able to identify electrodes selective for irrelevant locations, it was necessary for us to use an analytic method for identifying electrodes selective for each of the four target locations. The validity of this approach is demonstrated by the fact that it generates results with narrowband α (Fig. 6A) that are qualitatively similar to those generated with the conventional lateralized procedure (Fig. 2). (Note that quantitative

comparison of Fig. 2 vs Fig. 6A is complicated by the fact that Fig. 6A was generated with twice as many trials, because it also includes data from up/down blocks.)

These results are consistent with the idea that spatial selection is achieved, at least in part, via an increase in action potentials originating from the DAN and the pulvinar nucleus (Saalmann and Kastner, 2011). Although an effect of this activity is to synchronize local field potentials of targeted circuits with those generating these afferent signals (Levichkina et al., 2021), the resulting increase in spike-field coherence, whether prominent in the α band (Saalmann et al., 2012) or in other frequency bands (Mendoza-Halliday et al., 2014), is likely too small to detect with scalp EEG. Our results also suggest that the cue-locked macro-scale increase in α band power that is observed at unattended locations may be a secondary consequence of selection happening elsewhere, a return to an “idling” state similar to what is observed with eye closure. This interpretation is consistent with recent work that has concluded from careful measurement of the timing of attention-related changes in steady-state evoked potentials that changes in α band power measured at the scalp are too slow for them to have a direct role in attentional control (Antonov et al., 2020). It is important to note, however, that the results from other studies have been interpreted as evidence in favor of an active-inhibition function for α . For example, Schneider et al. (2019) explicitly entertain a secondary-consequence account of results from a working memory retrocuing task, but use logical argumentation to reject it in favor of an inhibitory account. Similarly, Rösner et al. (2020) also interpret retrocued-linked increases in α power to distractor inhibition. (See also a recent review from Woodman et al., 2021.) Future work that can incorporate the critical elements of the task design used here and from experiments such as Schneider et al. (2019) and Rösner et al. (2020) may be needed to adjudicate between these interpretations.

The results presented here are in line with the longstanding idea that spatial expectation about a forthcoming visual stimulus modulates α power in visual areas representing the attended location (Thut et al., 2006; Rihs et al., 2009). There is broad consensus that this decrease in α power does not correspond to merely a residual effect of the visual processing of the cue but that it reflects an endogenous modulation of posterior α that has the effect of increasing the excitability of visual circuits corresponding to the cued location. Furthermore, our results with decomposed components of the EEG signal confirm that this effect at the target of selection is truly specific to oscillations in the α band, because attended-unattended differences were observed in only the decomposed α signal, not in the aperiodic component of the EEG, which is also prominent at 8–14 Hz.

One novel aspect of our results is that they include a component of the EEG signal that has rarely been considered in attention research, but that does differentiate irrelevant from unattended locations: the slope of the aperiodic 1/f-like component. Because this measure is believed to reflect local cortical E:I balance (Freeman and Zhai, 2009; Voytek et al., 2015; Gao et al., 2017; Donoghue et al., 2020b; Ostlund et al., 2021; Waschke et al., 2021), this aspect of our findings gives us license to propose an attention-related mechanism that is different from shifts of selective attention. Knowledge that behaviorally relevant targets will only occur at specific locations in the visual field may prompt a tonic change in E:I balance at these locations, preconditioning them for anticipated target processing. This interpretation is also consistent with the recent observation that a cue to attend to a visual noise stimulus rather than to a concurrent auditory noise stimulus “result[ed] in a flattening of the EEG power spectrum over ... occipital electrodes” (Waschke et al., 2021).

We conclude with some methodological considerations. The combined use of univariate and multivariate analysis techniques allowed us to capitalize on the respective advantages of each, while avoiding many of their respective shortcomings. Univariate methods can produce measures that relate directly to brain physiology, such as functional differences between desynchronization and synchronization of oscillations in the α band (Thut et al., 2006; Romei et al., 2008a,b; Rihs et al., 2009; Capilla et al., 2014). A shortcoming of this approach, however, is that it often requires making a priori assumptions about “how the brain works,” as one does when selecting electrodes for a priori-defined ROIs. If any of these assumptions are incorrect, interpretation of the data will necessarily be flawed. Conversely, although multivariate techniques offer improved specificity, for example by weighting the contribution of various kinds of information across different features, they often produce measures without clear correspondence to observable physiological mechanisms. In the current study we used multivariate methods (LASSO and mIEM) to select electrodes whose activity was selective for only one of the four locations. This optimized the specificity of the signals that we measured and did not require us to assume that we know how up, right, down, and left are represented at the scalp. In particular, the loss function of the LASSO regularization procedure maximizes the contribution of location-informative channels while pushing to zero the contribution of nonrelevant and redundant channels (Tibshirani, 1996). Having so identified the ROIs, we then used a univariate approach (i.e., averaging across multiple electrodes to extract one signal per ROI) to assess fluctuations in physiological states (e.g., synchronization of LFPs, E:I balance) that are directly measurable. The improved sensitivity of this approach is evidenced by the presence of an earlier modulation of α

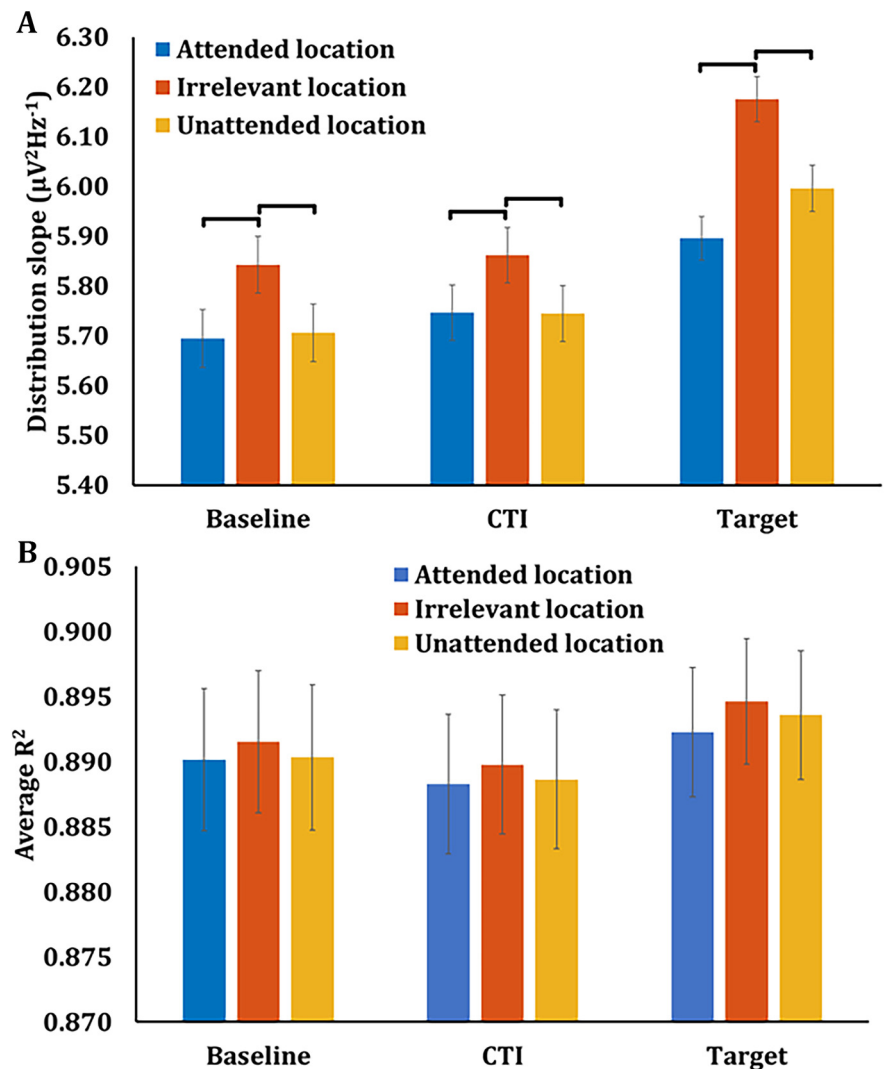


Figure 12. 1/f slope (A) and R^2 (B) from F000F parametrization across baseline (−500–0 ms), CTI (350–850 ms), and target presentation (850–1350 ms), from ROIs derived from multivariate analyses of 1/f slope data (Fig. 5). Black lines represent statistically significant comparisons (Newman–Keuls, $p \leq 0.05$).

power at the attended location in comparison to what has been observed using conventional lateralization procedures (Thut et al., 2006; Rihs et al., 2009). In our analyses, signals from a priori-defined lateralized ROIs did not show a statistically reliable cue-related modulation of α power until 1000 ms after cue onset, whereas from multivariate analysis-derived ROIs the same modulation was evident 380 ms after cue onset. The results with these multivariate analysis-derived ROIs are decidedly better aligned with behavioral estimates of the latency of endogenously triggered shifts of attention to a new spatial location (Müller and Rabbitt, 1989). Nonetheless, it must be acknowledged that this gain in sensitivity to temporal dynamics of the α signal comes at the expense of knowing where in the brain the signals were generated, a necessary consequence of the fact that neither LASSO nor mIEM are constrained by location-on-the-scalp of the signals that they process. For example, we cannot know the source of the signals that led to the incorporation of frontal scalp electrodes in some of the ROIs. One possibility is regions of frontal cortex that demonstrate retinotopic organization (Hagler and Sereno, 2006; Sprague and Serences, 2013; Mackey et al., 2017). Relatedly, in the macaque, local field potentials recorded from frontal eye field and supplementary

eye field have been shown to contribute to the contralateral delay activity (CDA), an event-related potential (ERP) component recorded at posterior electrodes that is associated with visuospatial attention and working memory (Reinhart et al., 2012).

References

- Antonov PA, Chakravarthi R, Andersen SK (2020) Too little, too late, and in the wrong place: alpha band activity does not reflect an active mechanism of selective attention. *Neuroimage* 219:117006.
- Berens P (2009) CircStat: a MATLAB toolbox for circular statistics. *J Stat Softw* 31:1–21.
- Capilla A, Schoffelen J-M, Paterson G, Thut G, Gross J (2014) Dissociated α -band modulations in the dorsal and ventral visual pathways in visuospatial attention and perception. *Cereb Cortex* 24:550–561.
- Cohen MX (2019) Analyzing neural time series data. Cambridge: The MIT Press.
- Corbetta M, Shulman GL (2002) Control of goal-directed and stimulus-driven attention in the brain. *Nat Rev Neurosci* 3:201–215.
- Delorme A, Makeig S (2004) EEGLAB: an open source toolbox for analysis of single-trial EEG dynamics including independent component analysis. *J Neurosci Methods* 134:9–21.
- Donoghue T, Dominguez J, Voytek B (2020a) Electrophysiological frequency band ratio measures conflate periodic and aperiodic neural activity. *eNeuro* 7:ENEURO.0192-20.2020.
- Donoghue T, Haller M, Peterson EJ, Varma P, Sebastian P, Gao R, Noto T, Lara AH, Wallis JD, Knight RT, Shestuyk A, Voytek B (2020b) Parameterizing neural power spectra into periodic and aperiodic components. *Nat Neurosci* 23:1655–1665.
- Dworkin JD, Linn KA, Teich EG, Zurn P, Shinohara RT, Bassett DS (2020) The extent and drivers of gender imbalance in neuroscience reference lists. *Nat Neurosci* 23:918–926.
- Efron B (1992) Bootstrap methods: another look at the jackknife. In: *Breakthroughs in statistics*, pp 569–593. New York: Springer.
- Foster JJ, Awh E (2019) The role of alpha oscillations in spatial attention: limited evidence for a suppression account. *Curr Opin Psychol* 29:34–40.
- Freeman WJ, Zhai J (2009) Simulated power spectral density (PSD) of background electrocorticogram (ECoG). *Cogn Neurodyn* 3:97–103.
- Gao R, Peterson EJ, Voytek B (2017) Inferring synaptic excitation/inhibition balance from field potentials. *Neuroimage* 158:70–78.
- Haegens S, Cousijn H, Wallis G, Harrison PJ, Nobre AC (2014) Inter- and intra-individual variability in alpha peak frequency. *Neuroimage* 92:46–55.
- Hagler DJ, Sereno MI (2006) Spatial maps in frontal and prefrontal cortex. *Neuroimage* 29:567–577.
- Jensen O, Mazaheri A (2010) Shaping functional architecture by oscillatory alpha activity: gating by inhibition. *Front Hum Neurosci* 4:186.
- Kelly SP, Lalor EC, Reilly RB, Foxe JJ (2006) Increases in alpha oscillatory power reflect an active retinotopic mechanism for distracter suppression during sustained visuospatial attention. *J Neurophysiol* 95:3844–3851.
- King-Smith PE, Grigsby SS, Vingrys AJ, Benes SC, Supowit A (1994) Efficient and unbiased modifications of the QUEST threshold method: theory, simulations, experimental evaluation and practical implementation. *Vision Res* 34:885–912.
- Klimesch W, Sauseng P, Hanslmayr S (2007) EEG alpha oscillations: the inhibition-timing hypothesis. *Brain Res Rev* 53:63–88.
- Levichkina E, Kermani M, Saalman YB, Vidyasagar TR (2021) Dynamics of coherent activity between cortical areas defines a two-stage process of top-down attention. *Exp Brain Res* 239:2767–2779.
- Mackey WE, Winawer J, Curtis CE (2017) Visual field map clusters in human frontoparietal cortex. *Elife* 6:e22974.
- Maris E, Oostenveld R (2007) Nonparametric statistical testing of EEG- and MEG-data. *J Neurosci Methods* 164:177–190.
- Mendoza-Halliday D, Torres S, Martinez-Trujillo JC (2014) Sharp emergence of feature-selective sustained activity along the dorsal visual pathway. *Nat Neurosci* 17:1255–1262.
- Mierau A, Klimesch W, Lefebvre J (2017) State-dependent alpha peak frequency shifts: experimental evidence, potential mechanisms and functional implications. *Neuroscience* 360:146–154.
- Müller HJ, Rabbitt PMA (1989) Reflexive and voluntary orienting of visual attention: time course of activation and resistance to interruption. *J Exp Psychol Hum Percept Perform* 15:315–330.
- Oostenveld R, Fries P, Maris E, Schoffelen JM (2011) FieldTrip: open source software for advanced analysis of MEG, EEG, and invasive electrophysiological data. *Comput Intell Neurosci* 2011:156869.
- Ostlund BD, Alperin BR, Drew T, Karalunas SL (2021) Behavioral and cognitive correlates of the aperiodic (1/f-like) exponent of the EEG power spectrum in adolescents with and without ADHD. *Dev Cogn Neurosci* 48:100931.
- Posner MI (1980) Orienting of attention. *Q J Exp Psychol* 32:3–25.
- Ramsøy TZ, Overgaard M (2004) Introspection and subliminal perception. *Phenomenol Cogn Sci* 3:1–23.
- Reinhart RMG, Heitz RP, Purcell BA, Weigand PK, Schall JD, Woodman GF (2012) Homologous mechanisms of visuospatial working memory maintenance in macaque and human: properties and sources. *J Neurosci* 32:7711–7722.
- Rihs TA, Michel CM, Thut G (2009) A bias for posterior α -band power suppression versus enhancement during shifting versus maintenance of spatial attention. *Neuroimage* 44:190–199.
- Romei V, Brodbeck V, Michel C, Amedi A, Pascual-Leone A, Thut G (2008a) Spontaneous fluctuations in posterior alpha-band EEG activity reflect variability in excitability of human visual areas. *Cereb Cortex* 18:2010–2018.
- Romei V, Rihs T, Brodbeck V, Thut G (2008b) Resting electroencephalogram alpha-power over posterior sites indexes baseline visual cortex excitability. *Neuroreport* 19:203–208.
- Rösner M, Arnau S, Skiba I, Wascher E, Schneider D (2020) The spatial orienting of the focus of attention in working memory makes use of inhibition: evidence by hemispheric asymmetries in posterior alpha oscillations. *Neuropsychologia* 142:107442.
- Saalman YB, Kastner S (2011) Cognitive and perceptual functions of the visual thalamus. *Neuron* 71:209–223.
- Saalman YB, Pinsk MA, Wang L, Li X, Kastner S (2012) The pulvinar regulates information transmission between cortical areas based on attention demands. *Science* 337:753–756.
- Sadaghiani S, Kleinschmidt A (2016) Brain networks and α -oscillations: structural and functional foundations of cognitive control. *Trends Cogn Sci* 20:805–817.
- Samaha J, Sprague TC, Postle BR (2016) Decoding and reconstructing the focus of spatial attention from the topography of alpha-band oscillations. *J Cogn Neurosci* 28:1090–1097.
- Schneider D, Göddertz A, Haase H, Hickey C, Wascher E (2019) Hemispheric asymmetries in EEG alpha oscillations indicate active inhibition during attentional orienting within working memory. *Behav Brain Res* 359:38–46.
- Sprague TC, Serences JT (2013) Attention modulates spatial priority maps in the human occipital, parietal and frontal cortices. *Nat Neurosci* 16:1879–1887.
- Thut G, Nietzel A, Brandt SA, Pascual-Leone A (2006) Alpha-band electroencephalographic activity over occipital cortex indexes visuospatial attention bias and predicts visual target detection. *J Neurosci* 26:9494–9502.
- Tibshirani R (1996) Regression shrinkage and selection via the lasso. *J R Stat Soc Ser B* 58:267–288.
- Voytek B, Kramer MA, Case J, Lepage KQ, Tempesta ZR, Knight RT, Gazzaley A (2015) Age-related changes in 1/f neural electrophysiological noise. *J Neurosci* 35:13257–13265.
- Waschke L, Donoghue T, Fiedler L, Smith S, Garrett DD, Voytek B, Obleser J (2021) Modality-specific tracking of attention and sensory statistics in the human electrophysiological spectral exponent. *Elife* 10:e70068.
- Watson AB, Pelli DG (1983) Quest: a Bayesian adaptive psychometric method. *Percept Psychophys* 33:113–120.
- Welch PD (1967) The use of fast Fourier transform for the estimation of power spectra: a method based on time averaging over short, modified periodograms. *IEEE Trans Audio Electroacoust* 15:70–73.
- Woodman GF, Wang S, Sutterer DW, Reinhart RMG, Fukuda K (2021) Alpha suppression indexes a spotlight of visual-spatial attention that can shine on both perceptual and memory representations. *Psychon Bull Rev* 1:1–18.
- Zar JH (1999) *Biostatistical analysis*. Upper Saddle River: Prentice Hall.